Electronic Supplementary Material (ESI) for Nanoscale.

Supplementary Materials

Enabling Sequential Rupture for Lowering Atomistic Ice Adhesion

Senbo Xiao*[a], Bjørn Helge Skallerud[a], Feng Wang[a], Zhiliang Zhang[a] and Jianying He*[a]

[a] NTNU Nanomechanical Lab, Department of Structural Engineering, Norwegian University of Science and Technology (NTNU), 7491 Trondheim, Norway

Supplementary Figures

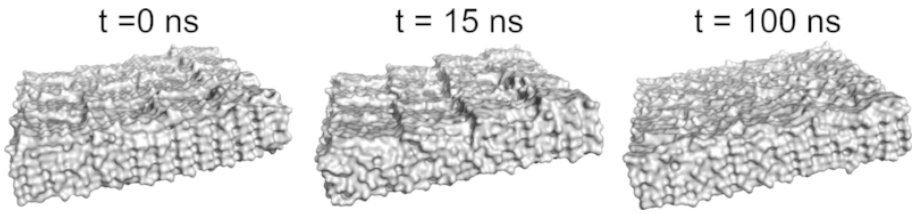

Supplementary Figure S1: **Changes in the contacting surface topography of ice after adhering simulation and during shearing against the tilting direction of graphene platelets.** The contacting surface of the ice were shown upward in all the snapshots at different shearing simulation time of the same trajectory. The face of the ice matched with the topography of the fish-scale-like surface after the adhesion simulation (left panel, $t = 0$ ns). The roughness of the contacting surface shown significant increase from $t = 0$ ns to 15 ns, and then smoothed out at the end of the simulation at 100 ns.

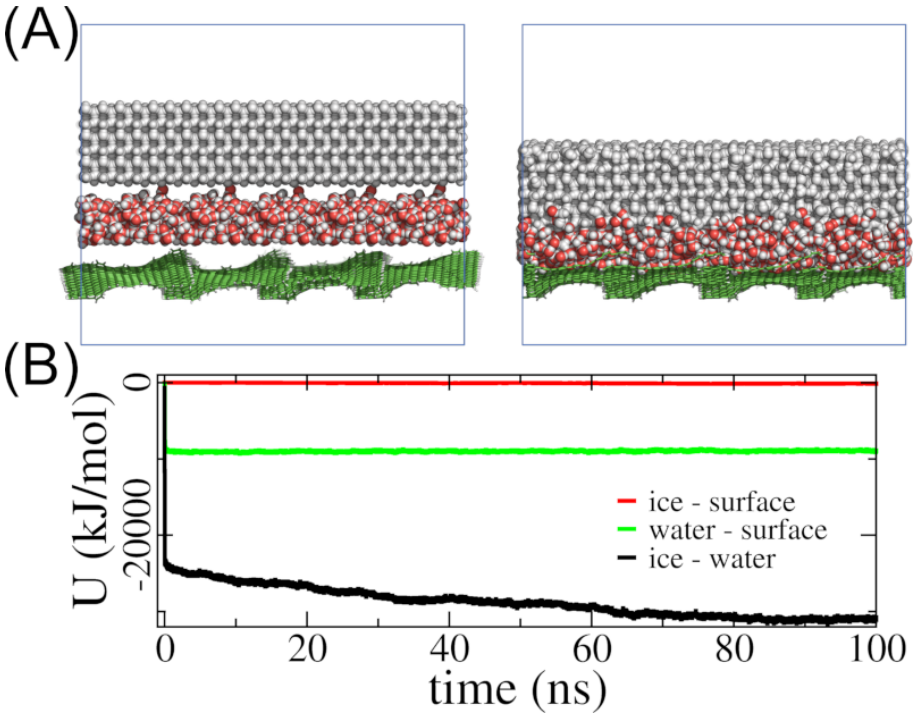

Supplementary Figure S2: **Ice adhered onto the fish-scale-like surface with a sandwiched layer of lubricating water.** (A) Snapshots of the system at the beginning (left, t = 0 ns) and the end (right, t = 100 ns) of the ice adhesion simulation. (B) Atomistic interactions, Lennard-Jones potential, between the ice, the water layer and the surface in the course of 100 ns ice adhesion simulation. The water layer in this system had a thickness of 1 nm. The atomistic interactions between the ice and the water layer included Lennard-Jones and electrostatics potentials. The interactions between the surface and the ice or the water layer were Lennard-Jones potential, given that the surface atoms were electrically neutral.

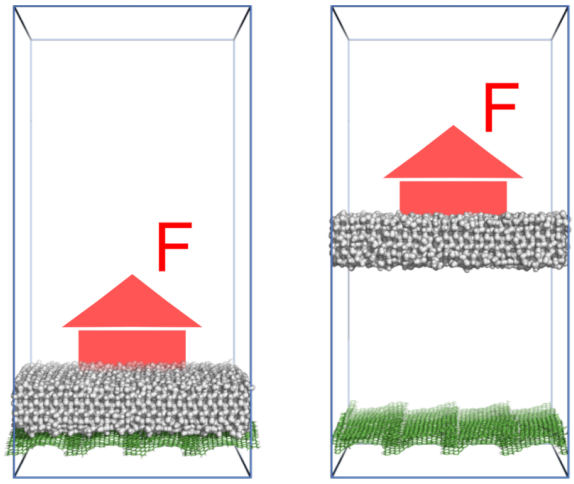

Supplementary Figure S3: **Ice concurrent rupture from the fish-scale-like surface.** System snapshots showed ice before and after the rupture event on the left and the right panels, respectively.

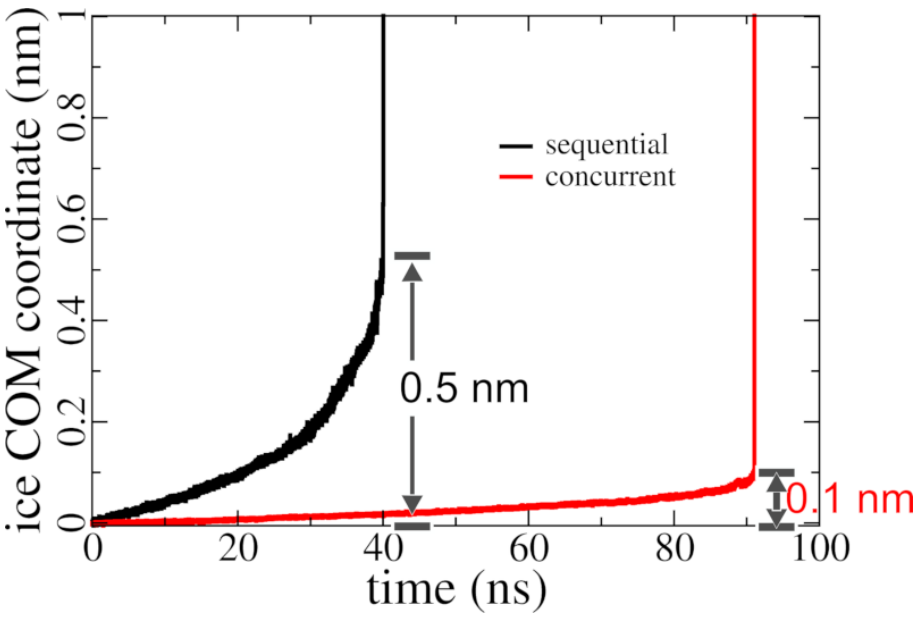

Supplementary Figure S4: **Examples of COM coordinate of the ice in rupture simulations, showing energy depth of 0.1 nm and 0.5 nm for concurrent and sequential rupture modes, respectively.**

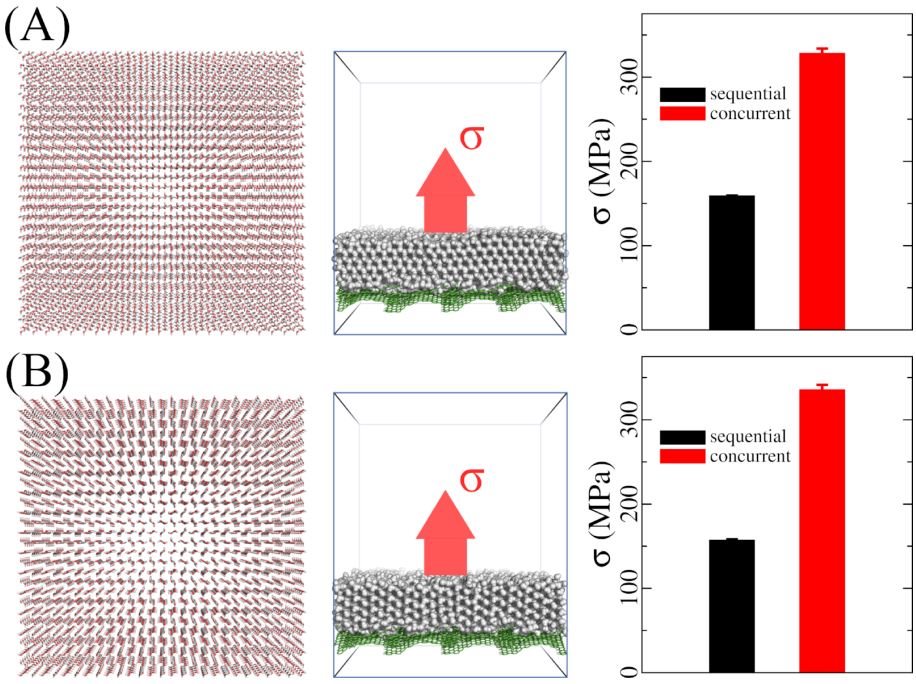

Supplementary Figure S5: **Sequential and concurrent rupture of different ice faces.** (A) I_h model with the prism face for adhesion. The initial structure of the ice is on the left panel, with top view of the initial prism adhesion face. The ice adhered onto the fish-scale surface for 100 ns, and was subjected to pulling force as indicated in the middle panel. All the simulations use the same parameters given in the Method section in the main text. Sequential and concurrent rupture stresses of the prism face on the right panel were obtained from three indepedent runs, which were 159.19±0.38 MPa and 328.40±5.41 MPa, respectively. The error bars indicate standard deviations. (B) I_h model with the second prism face for adhesion for comparison with prism face in (A). Sequential and concurrent rupture stresses of the second prism face monitored were 157.21±0.93 MPa and 335.68±5.83 MPa, respectively.

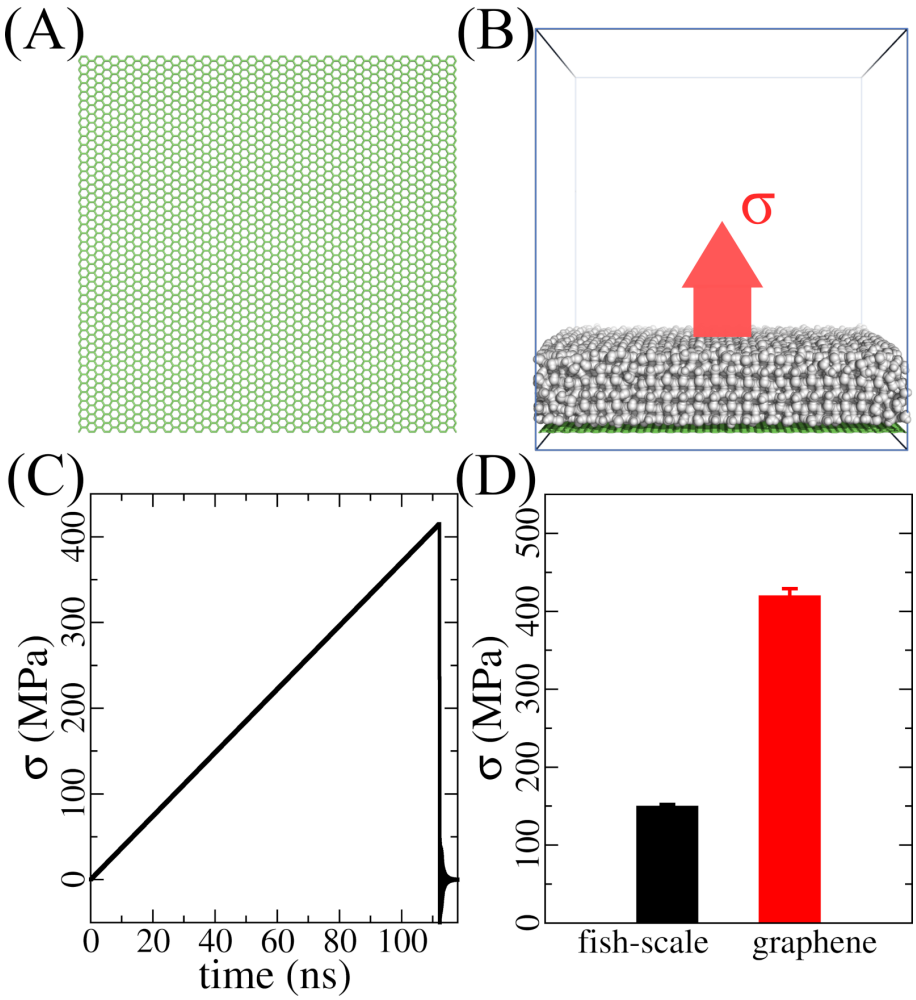

Supplementary Figure S6: **Detaching ice from flat graphene surface.** (A) Periodic graphene surface for ice adhesion. The graphese has the same area with the adhesion face of the ice model used in the main text. (B) The same ice model as in Fig.4 stabily adhered on the graphene after 100 ns equilibrating simulation. The red arrow in the figure indicates the direction of the applied stress. (C) Typical stress profile obtained in detaching ice from the graphene observed in 3 indepedent runs using the same simulation parameters as detaching ice from the fish-scale surface. (D) Ice detaching stress monitored on the graphene (in red, 417.63±9.38 MPa) and compared to sequential rupture stress on the fish-scale surface(in black, 149.75±2.35 MPa), with error bars showing standard deviations. The graphene has similar surface energy, G in Eqn.(1) in the main text, with the fish-scale surface, yet shows much higher ice detaching stress owing to lack of sequential rupture.

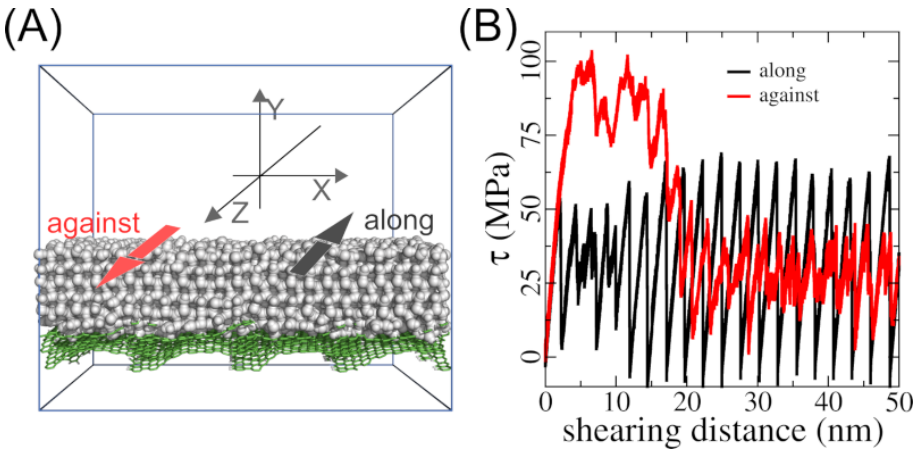

Supplementary Figure S7: **Shearing ice on the fish-scale-like surface on the Z-axis of the simulation box.** (A) System snapshot for the shearing simulation, with its coordination system and indications of the shearing direction. (B) Ice shearing stress profiles observed in the course of simulations.

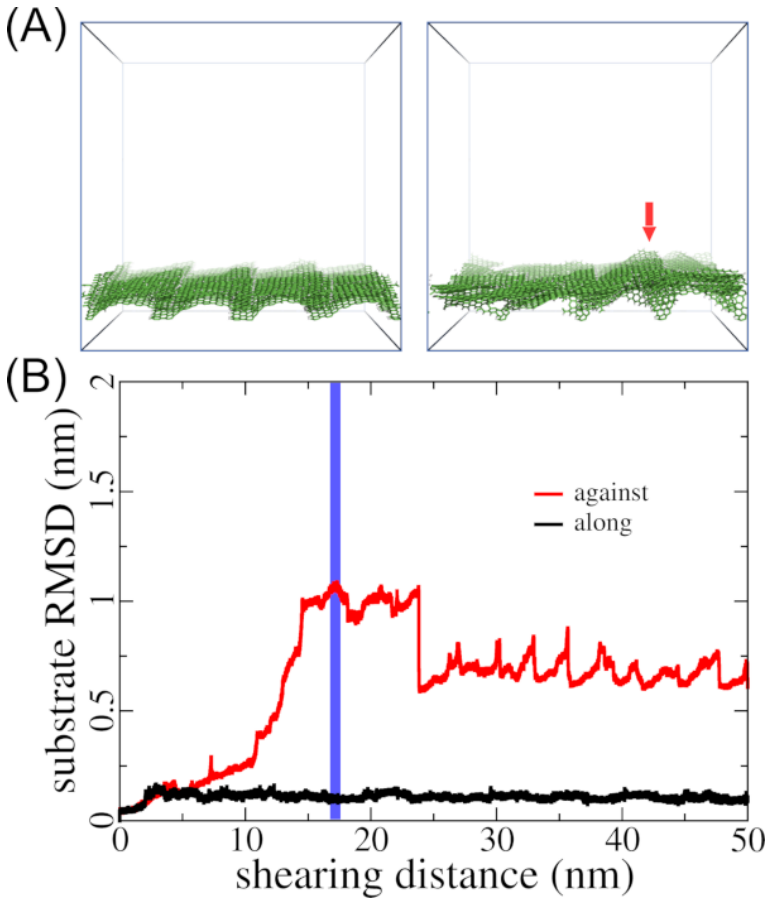

Supplementary Figure S8: **Morphology of the fish-scale-like substrate under shearing.** (A) Example snapshots of the fish-scale-like substrate under shearing stress along (left) and against (right) the graphene orientation direction. The red arrow indicates the graphene platelets that are in bending and buckling geometries. (B) Structural root-mean-squared deviation (RMSD) of the substrate in the course of shearing simulations. $RMSD = \sqrt{\frac{1}{N}\sum_{n=1}^{N}(r_i^2 - r_0^2)}$, where N is the total number of atoms in the substrate, r_0 and r_i are coordinates of the atoms in the initial and the sheared snapshots. The blue color bar indicates when the snapshots in (A) were taken.

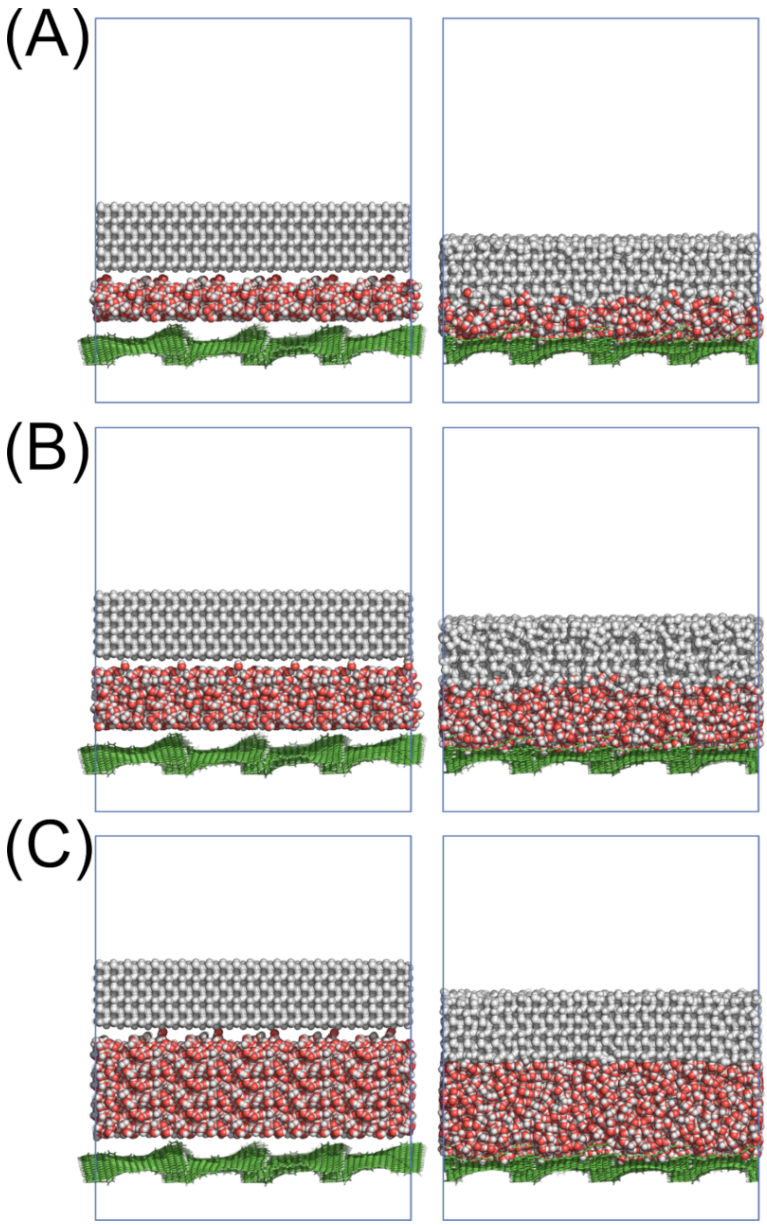

Supplementary Figure S9: **Ice adhesion on the fish-scale-like surface with interfacial water layers.** The initial (left panel) and fully adhered (100 ns, right panel) models of interfacial water layers with thickness 1, 2 and 3 nm were showed in (A), (B) and (C), respectively.

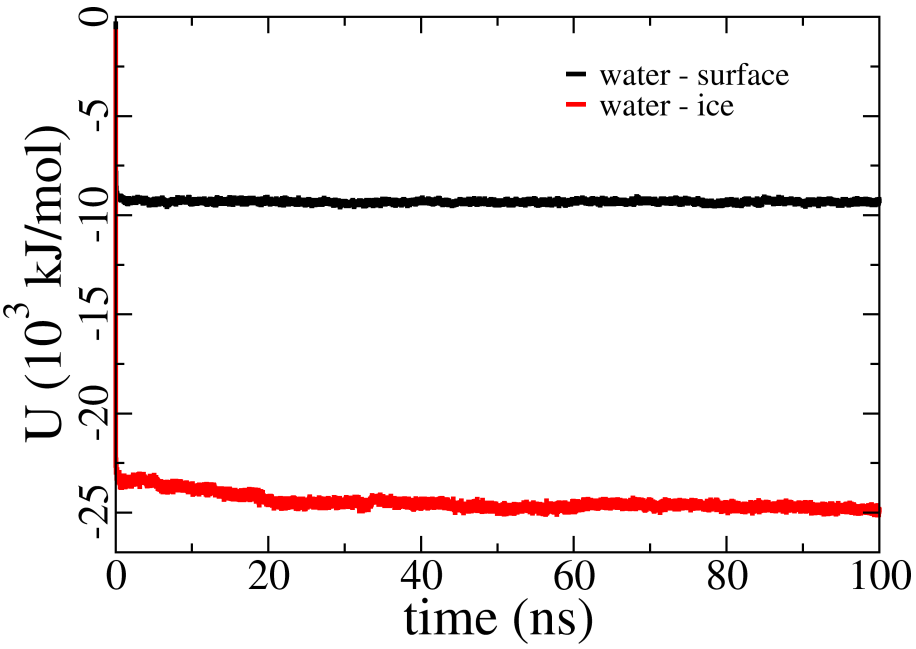

Supplementary Figure S10: **Interaction potential of the interfacial water layer with the surface and ice in the ice adhesion simulation of 100 ns.**

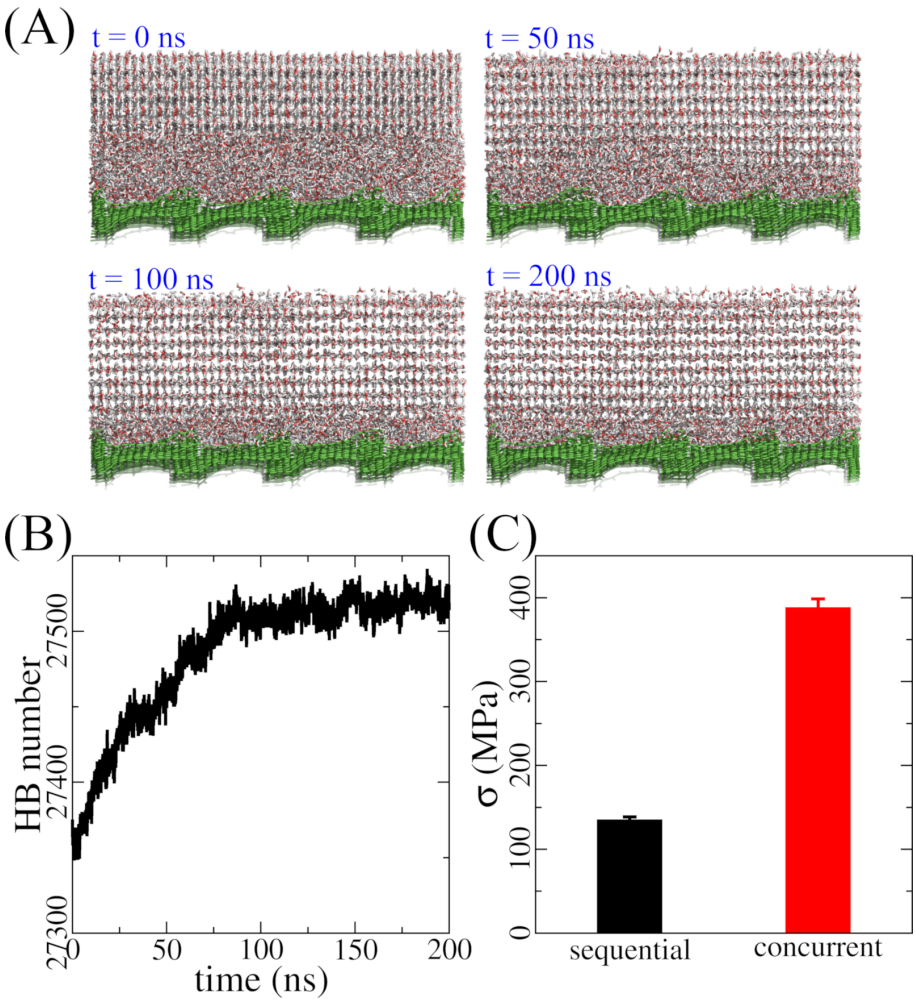

Supplementary Figure S11: **Freezing of the interfacial water and the resulted adhesion stresses at two rupture modes.** (A) System snapshots of ice growth in 200 ns. The temperture of the 2-nm water layer was set to the same as the ice in ths simulation. The simulation time of the snapshot was highlighted in the figures. Ice grew from the original ice layer and reached the fish-scale-like surface in the end of 200 ns simulations. The ice structure in the grooves of the surface was amouphous, and stable in the second half of the simulation. (B) The hydrogen bond (HB) number monitored among the water molecules in the 200 ns ice growth simulation. The HB number stabily increased in the first half of the simulation, showing the growth of the ice structure in the system. After the ice reaching the fish-scale-surface, the HB number maintained a stable value in the second half of the simulation. (C) Sequential and concurrent ice rupture stress after the ice growth simulation. The system snapshot at 200 ns of the ice growth simulation was taken for ice detaching simulation, using the same simulation parameters given in the method section of the main text. The Sequential and concurrent rupture stress were 134.8±3.8 and 388.0±10.6 MPa, respectively, with standard deviation from 3 indenpent runs. The result further confirms the outperforming low ice adhesion strength by the sequential rupture mode.

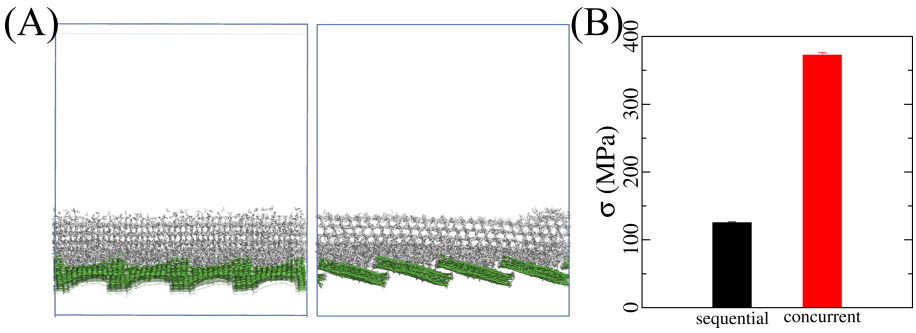

Supplementary Figure S12: **Sequential and concurrent rupturing ice formed on the fish-scale-like surface.** (A) Snapshots at different viewing angles of the newly formed ice on the fish-scale-like surface. The system used for this simulation was taken from Suppl.Fig. S11 by deleting the original ice top layer. The newly ice structure was then subjected to detaching force using the same pulling simulation parameters. (B) Sequential and concurrent ice adhesion strength of the the newly formed ice, which were 125.4±1.1 MPa and 372.4±3.9 MPa, respectively. The concurrent rupture stress featured high ice adhesion strength similar to ice rupture from flat graphene (Suppl.Fig. S6), while the sequential rupture stress was much lower.

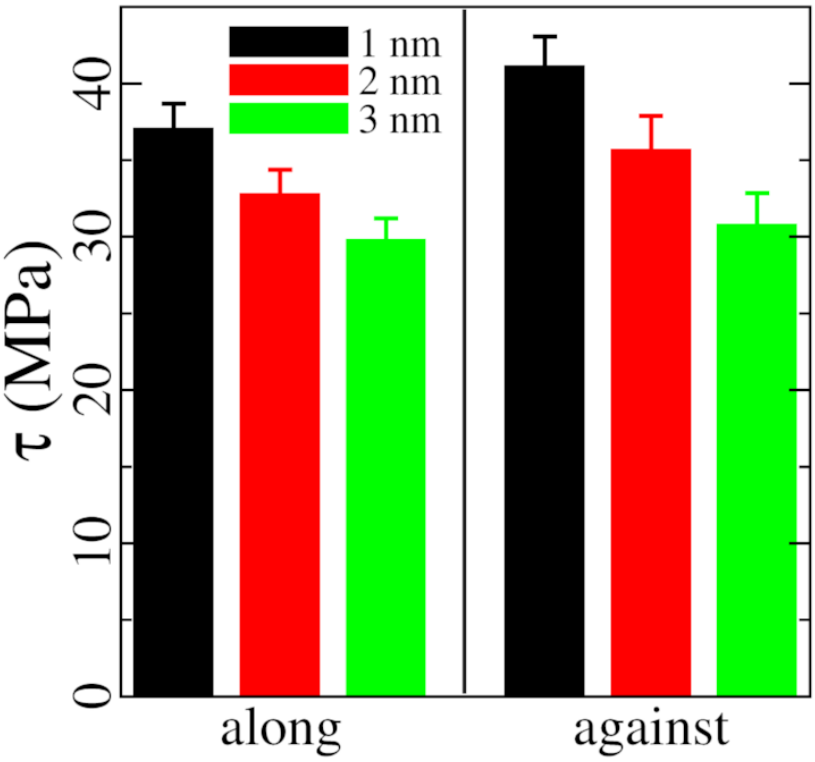

Supplementary Figure S13: **Average ice shearing stress with different thickness of lubricating water layers.** The average shearing stress were obtained at the second half of the shearing simulations on the Z-axis of the simulation box, both along and against the graphene tilting orientation. The thickness of the lubricating water layers is indicated by the legends. The error bars show standard deviations in each dataset.

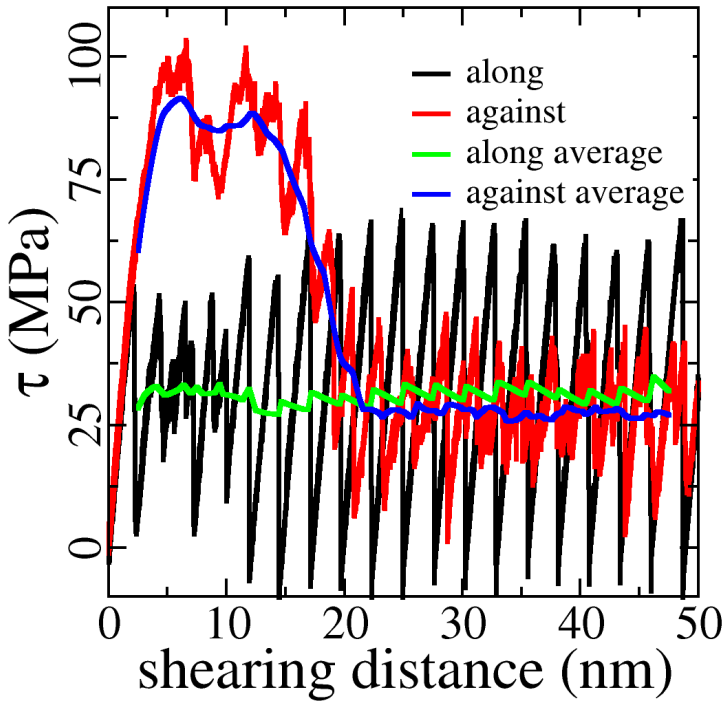

Supplementary Figure S14: MD simulation results for shear loading, and corresponding average curves.

Basic mechanical models for graphene-ice structural response in tension or shear

Suppl.Fig. S14 shows the main characteristics of the stress versus displacement response for the ice block subjected to global sliding to the right (along) and to the left (against). It is noted two main features. First, the response is very dynamic, with a very nonlinear curve. One reason for this peak and valley response is due to the cohesion-decohesion between the graphene and the ice. Second, there is a significant difference between the response in sliding to the left and to the right. This is clearly shown when comparing the average response curves also. For the left movement, the stress reaches a global peak followed by a reduction that finally approaches the response obtained for the movement to the right. Subsequently, some simple mechanics approaches are employed to point out qualitatively some different mechanisms that evolve in the two loading directions. First, the mode 1 tensile response is addressed, followed by the two shear sliding mode 2 responses.

The system is simplified to consist of a rigid block of ice and a rigid substrate. The connection between these is obtained by straight graphene sheets with an angle α with respect to the horizontal plane. The graphene sheet is simplified as a straight planar beam element. Considering a planar beam finite element, it has 6 degrees of freedom (DOF), three at each end. Denoting the DOF as $[v_1, v_2, v_3, v_4, v_5, v_6]^T$, where the superscript T denotes the transpose of the vector, the relation between the end forces and moments

and the DOF is given by the stiffness matrix $\mathbf{k}$:

$$\begin{bmatrix} \mathbf{S_1} \\ \mathbf{S_2} \end{bmatrix} = \begin{bmatrix} EA/L & 0 & 0 & -EA/L & 0 & 0 \\ 0 & 12EI/L^3 & -6EI/L^2 & 0 & -12EI/L^3 & -6EI/L^2 \\ 0 & -6EI/L^2 & 4EI/L & 0 & 6EI/L^2 & 2EI/L \\ -EA/L & 0 & 0 & EA/L & 0 & 0 \\ 0 & -12EI/L^3 & 6EI/L^2 & 0 & 12EI/L^3 & 6EI/L^2 \\ 0 & -6EI/L^2 & 2EI/L & 0 & 6EI/L^2 & 4EI/L \end{bmatrix} \begin{bmatrix} v_1 \\ v_2 \\ v_3 \\ v_4 \\ v_5 \\ v_6 \end{bmatrix} \quad (1)$$

$$= \begin{bmatrix} \mathbf{k_{11}} & \mathbf{k_{12}} \\ \mathbf{k_{21}} & \mathbf{k_{22}} \end{bmatrix} \begin{bmatrix} \mathbf{v_1} \\ \mathbf{v_2} \end{bmatrix} \quad (2)$$

Here L is length of graphene sheet, E is Young's modulus, A is cross section area, and I second area moment. The beam element is at an angle and the DOF is defined in the local coordinate system. The global DOF are defined in the global coordinate system (i.e. the displacements at the end of the beam are in the horizontal and vertical direction). The link between the global and local DOF can be expressed by means of transformation matrices: $\begin{bmatrix} \mathbf{r_1} \\ \mathbf{r_2} \end{bmatrix} = \begin{bmatrix} \mathbf{T_0} & \mathbf{0} \\ \mathbf{0} & \mathbf{T_0} \end{bmatrix} \begin{bmatrix} \mathbf{v_1} \\ \mathbf{v_2} \end{bmatrix}$, where $\mathbf{T_0} = \begin{bmatrix} \cos\alpha & -\sin\alpha & 0 \\ \sin\alpha & \cos\alpha & 0 \\ 0 & 0 & 1 \end{bmatrix}$. α is the angle of the beam with respect to the horizontal axis.

We assume that the beam is constrained with respect to all global DOF except the vertical displacement at the node attached to the (rigid) ice. With this the graphene beam has the following global stiffness: $k = k_{44}\sin^2\alpha + k_{55}\cos^2\alpha$. Now we introduce a cohesive element between the upper beam node and the ice. With this, the resistance to vertical displacement is obtained as a result of the beam displacement and the displacement from the cohesive element (i.e they act in series). The cohesive zone response is modeled as simple as possible: An initial rigid response up to a maximum load F_{max} followed by a linear decrease in load until a maximum displacement δ_{max} is reached. After this, the cohesive element does not carry any load.

Consider a centrally applied load P to the ice. Then all graphene sheets will be subjected to the same vertical displacement and all n beam elements in the calculation domain respond to this displacement. The total stiffness reads $K = n \cdot k$. The maximum vertical force that can be applied is governed by the n cohesive elements, i.e. $P_{max} = n \cdot F_{max}$. Denoting the horizontal extension of the ice as $2a$, we can smear out the discrete graphene elastic stiffness and cohesive element force over this length: $k := \frac{K}{2a}$ and $F_{max} := \frac{n \cdot F_{max}}{2a}$. Hence, the global elastic response of the system is $P = 2ak\Delta$, where Δ is the global vertical displacement of the ice block. The maximum load reads $P_{max} = 2aF_{max}$.

Now we consider that the ice block is subjected to a global load applied eccentrically at the left corner. Assuming that the block is rigid, the block will rotate around the lower right point of the block (which is in contact with the rigid substrate). This leads to a linear displacement field $\delta(x)$ along the graphene layer, with zero value at the right side and a maximum equal to the global displacement Δ at the left side (where the global load is applied). Hence, $\delta = \Delta(1 - \frac{x}{2a})$. The elastic response is now a function of x: $F = k\delta$. Taking moment equilibrium of the ice block we have $P \cdot 2a = \int_0^{2a} F(2a - x)dx$. Hence, the global stiffness reads $P = \frac{5}{6}ak\Delta$. Crack initiation happens when $\Delta = \frac{F_{max}}{k}$. This leads to the maximum global load $P_{max} = \frac{5}{6}aF_{max}$.

From these two simplified analyses (either the global load applied centrally in the ice block, or applied eccentrically at the edge of the block), a significant difference in stiffness and capacity is obtained: $k_{central}/k_{eccentric} = 2/(5/6) = 2.4$, $P_{max,central}/P_{max,eccentric} = 2/(5/6) = 2.4$.

If we do not smear out the graphene stiffness and cohesive element strength, but employ the data used in the MD simulations (i.e. 4 graphene sheets in the domain), the same stiffness ratio and strength ratio between central and eccentric global loading are obtained.

Now we consider the shear loading case. For this loading case the ice block is moving horizontally,

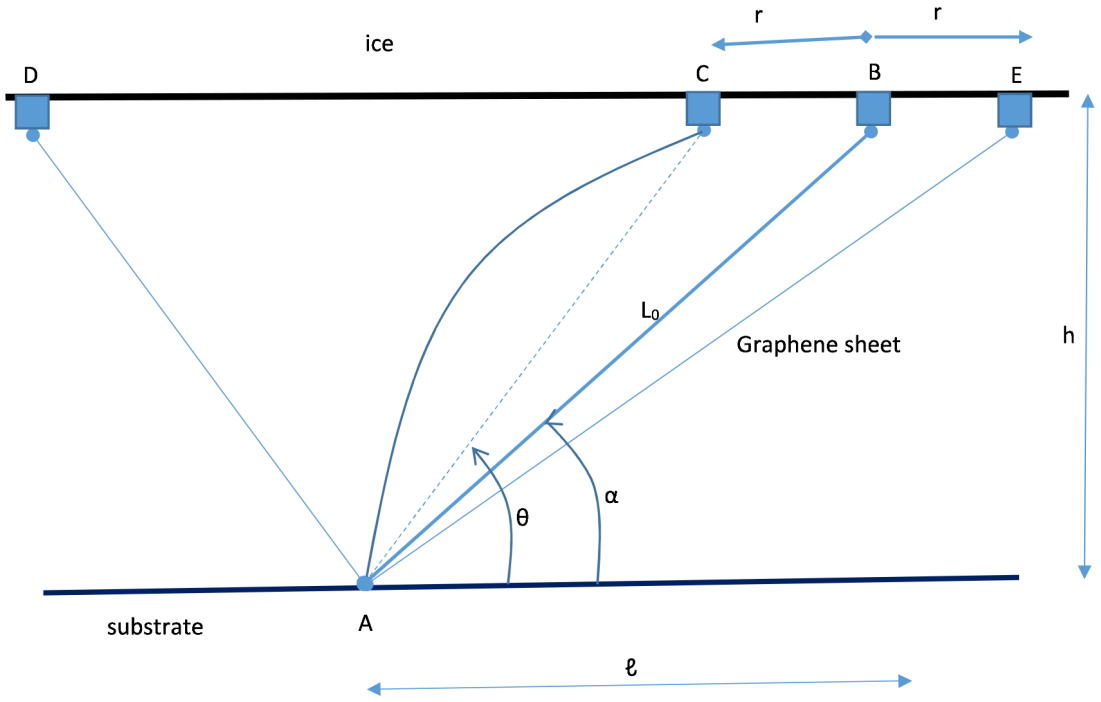

Supplementary Figure S15: Ice-graphene-substrate system. Initial unloaded configuration, AB; deformed configuration for global displacement to the right, AE; intermediate buckled configuration for global displacement to the left, AC; new reference configuration when global displacement has moved all the way to D. Height h is kept constant.

either to the left and to the right. The vertical distance between the ice and the substrate is kept constant. For illustration purpose the initial reference (unloaded) configuration of the graphene is set to an angle $\alpha = 45$ degrees, see Suppl.Fig. S15. Also, we assume the graphene sheets are unconstrained with respect to rotations at each end. Hence, the axial stiffness (EA/L_0) governs the elastic stiffness of the sheets. In the figure the small square at the upper node of the sheet element represents a cohesive element that carries the shear load. This cohesive element is assumed to follow a simple linear elastic-perfectly plastic shear response.

If we consider moving the block to the right, a tension force develops in the graphene sheet. The axial stiffness of the graphene sheet is high and the sheet strength is much higher than the cohesive capacity (the square element in the figure). Hence, in this case the global shear load pointing to the right almost instantly reaches a level corresponding to shear yielding in the cohesive element. The elastic stiffness of the sheet is found as follows. The axial force in the sheet is related to the elongation of the sheet: $N_{AE} = \frac{EA}{L_0}\Delta_{AE}$. Here the subscript AE corresponds to the letters in the figure (i.e. the end points of the sheet). Accounting for large transverse global displacement denoted r, the horizontal reaction force due to the tension in the sheet reads: $N_r = N_{AE}\cos\theta = \frac{EA}{L_0}(L_{AE} - L_0)\frac{\ell + r}{L_{AE}} = EA(1 - \frac{1}{\sqrt{1+\frac{r}{\ell}+0.5(\frac{r}{\ell})^2}})0.71(1+\frac{r}{\ell})$. This function has a slight nonlinearity, with increasing stiffness for larger global displacement to the right.

Considering the global displacement to the left, one scenario is that the graphene sheet buckles. The global displacement leads to compression in the beam, and due to the large axial stiffness (as described above for tension), the compressive force builds up quickly with only marginal global displacement. The Euler buckling load reads $N_E = \frac{\pi^2 EI}{L_0^2}$. Hence, it is reasonable to assume that when the global displacement

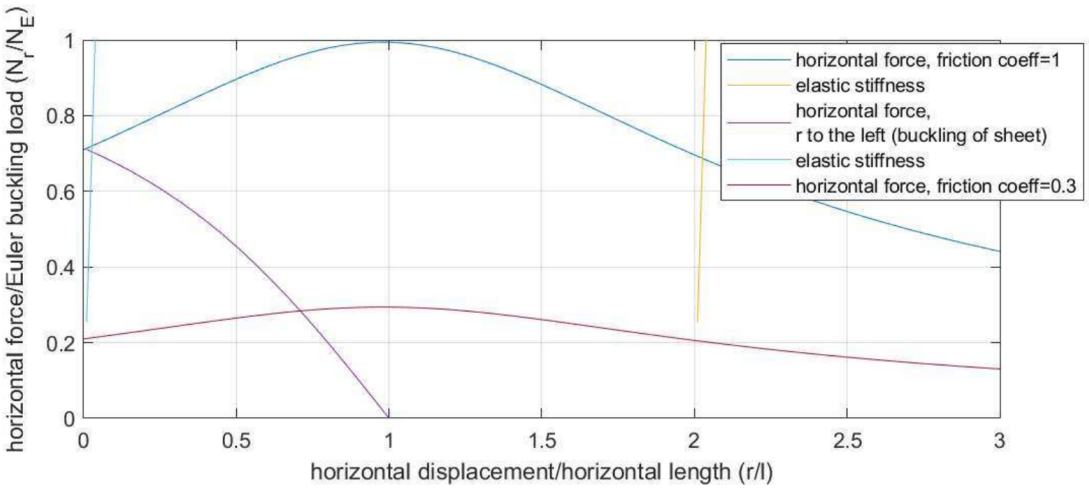

Supplementary Figure S16: Normalized horizontal load versus normalized horizontal displacement.

evolves to the left, the sheet is in its elastic buckled state. In Fig. S13 this is illustrated by the curved line between points A and C. It is of interest to investigate the response for a displacement from intital state (point B) to state D. At D $r = 2\ell$ and further displacement leads to tension in the sheet, with a response similar to the one described above for tension (i.e. point B moves to point E). This means that, for fixed distance between ice and substrate (h), the transverse displacement for the buckled sheet is large. The response of buckled columns with large displacement is found from elastica theory (see e.g. Timoshenko). It turns out that for quite large deformations of the buckled column, the axial load is almost constant, however the axial load increases somewhat for increasing displacement. We assume that the axial load in the local sheet element system is constant and equal to N_E. This simplifies the analysis. The horizontal force component from the buckled sheet reads $N_r = N_E \cos\theta = N_E \frac{\ell - r}{\sqrt{h^2+\ell^2-2\ell r+r^2}} = N_E \frac{1-\frac{r}{\ell}}{\sqrt{(\frac{L_0}{\ell})^2-2\frac{r}{\ell}+(\frac{r}{\ell})^2}}$. Using the initial angle of 45 degrees, $\frac{L_0}{\ell} = \sqrt{2}$. Plotting this response function (Fig.S14), normalizing the horizontal force with respect to the Euler buckling load (N_r/N_E) the load reaches the buckling load at zero transverse displacement, then a decrease in the horizontal force evolves until r/ℓ=1 , where the resistance to horizontal displacement is zero. Increasing the global displacement slightly we have an unstable system (the horizontal force starts to act in the opposite direction), and the system will snap to configuration AD (i.e. r/ℓ=2). Now the load can increase again due to the tension force developing in the sheet, similarly as for the case when point B moves to E. It can be remarked that in order to plot the linear elastic stiffness in tension in the plot normalized by N_E, one needs to calculate the ratio between EA and $\pi^2 EI/L_0^2$. Therefore actual dimensions must be used. In our case the length of the graphene sheet is approximately 2.3 nm and the thickness 0.3 nm. With this the ratio is obtained as 71, i.e. illustrating the high axial stiffness for the unbuckled state.

So far the influence of the cohesive element has not been considered. Assume that the cohesive force follows an Amontons-Coloumb friction law: $F = \mu N$. The normal force N is a result of the axial force in the sheet, i.e. $N = N_E \sin\theta$. Two almost horizontal lines are plotted in Fig.S14, the upper corresponds to $\mu = 1$, the lower $\mu = 0.3$. The slight variation for varying r/ℓ is due to the $\sin\theta$ term. If the maximum friction force is larger than the horizontal force corresponding to buckling , then the buckling response governs the ice-graphene response. Then, after buckling initiates, the horizontal load must decrease, the sheet snaps from r/ℓ=1 to r/ℓ=2 at zero load, followed by increasing load again. If the maximum friction force is smaller than the horizontal force corresponding to buckling of the sheet, the sheet never buckles,

and the response is governed by the sliding in the cohesive element. One can expect that the friction force will be higher when the sheet is in compression than in tension. Hence, the two curves corresponding to $\mu = 1$ and 0.3 can represent this.

Considering global displacement to the right, one can expect a global horizontal load steeply increasing to the level corresponding to shear sliding in the cohesive element. This corresponds to the response in Fig. S14 given by the green (average) curve. For global displacement to the left, one can expect the sliding capacity increases to a level higher than the force corresponding to sheet buckling. Hence, the sheet buckles first, the horizontal load decreases to zero, and starts to increase in a similar manner as for r moving to the right when the snap to point D is reached. This response differs from the average (blue) curve in Fig. S14. The initial response, going linearly to a maximum followed by a decrease, correponds to Fig. S14. However, in Fig. S14 the load does not reduce to zero. One reason for this post-collapse deviation is that in the simple approach all of the graphene sheets buckles simultaneously (followed by a snap through). In the MD simulation, random variations in boundary conditions and initial configurations prevent the graphene sheets to collapse simultaneously. Hence, one sheet may be in a buckled state, the others not. This leads to a load carrying capability and a smoother global average response in the post-collapse region.